

Eulerian space-time correlations in turbulent shear flows

W. R. C. Phillips wrphilli@uiuc.edu

Department of Theoretical and Applied Mechanics

University of Illinois at Urbana-Champaign, Urbana, IL 61801-2935, USA.

(March 30, 2000)

Abstract

This paper is concerned with the generic form of space-time correlations of instantaneous velocity fluctuations in turbulent shear flows. The study has as its basis the Kovasznay-Corrsin conjecture modified to account for inhomogeneities. Details of the modifications were dictated by comparison with DNS simulations of turbulent channel flow. For example, analysis of the simulations shows that the space-time correlations at optimal delay depict, when appropriately normalized, a form independent of turbulence component. It is also evident that the half width of the correlation grows, in the outer region of the layer, like V^{n+1} , while the Lagrangian time scale grows like V^n , where $2 < n < 3$ and V is the mean convection velocity. The resulting generic form for the space-time correlation captures these effects well and brings to light a Reynolds number effect that is most evident in the tail of the correlations at non-optimal delay.

I. INTRODUCTION

Correlations of the instantaneous velocity separated in space and time in turbulent shear flows have long been recognized to contain a wealth of information about the underlying structure of the flow [1] and consequently form the basis of methods to deduce that structure. Such methods include proper orthogonal decomposition [2,3], linear stochastic estimation [4]) and mean field theory [5–10]. All methods are in their infancy, but to further exploit them requires knowledge of R_{ij} for various space and time separations (see Sec. VII) for all space in the shear layer.

Measurements of space-time correlations have been made in boundary layers [11], pipe flow [12] and axisymmetric jets [13]. Kim & Hussain [14,15] (henceforth KH, or KH1 and KH2 respectively) have also extracted them from Kim, Moin & Moser’s [16] low Reynolds number DNS of channel flow.

Unfortunately the acquisition of space-time correlations is time and storage intensive. In consequence none of the studies can be considered complete, vis a vis providing $R_{ij}(\mathbf{x}; \mathbf{r}, \tau)$ correlations over all space \mathbf{r} and time τ separations for all space \mathbf{x} of interest. Acquisition of R_{ij} is further hampered by constraints such as probe interference in experiments and numerical limitations in DNS. A relevant question, therefore, is whether a credible interpolative basis can be constructed to bridge the gap between measured or calculated correlations, and that is the aim of this paper.

Such a concept was first conceived in the context of homogeneous, isotropic turbulence and was realized with some success by Favre [17] on the basis of the Kovasznay-Corrsin conjecture [18,19]. Our intent here is to explore whether the conjecture remains useful in non-homogeneous, non-isotropic turbulent flows.

We find in fact that the conjecture, which states that the space-time correlation can be expressed in terms of the space correlation and its probabilistic diminution with time (see Sec. II), is meaningful, at least for the purposes of modeling. And, perhaps more importantly, we find that complicating features like non-homogeneity and non-isotropy can

be factored away; this is seen most clearly in the context of correlations at optimal delay (Secs. III). On the other hand, space time correlations at non-optimal delay (Sec. IV) are found to be Reynolds number dependent, at least in the tail of the correlation.

As a basis for comparison we use the DNS results of KH. These results are not of course affected by probe effects, but it is unwise to assume direct simulations readily admit a plethora of credible estimations of $R(\mathbf{x}; \mathbf{r}, \tau)$; they do not. Indeed special runs with reduced time and spatial steps were necessary to ensure the realization of credible statistics. Furthermore, credibility of these statistical quantities is limited to \mathbf{r} -spacings less than about a quarter of the fundamental streamwise Fourier wave length employed in the calculation, which translates to about 1000 wall units. Subsequent calculations of $R(\mathbf{x}; \mathbf{r}, 0)$ have been made by Moser, Kim & Mansour [20] although calculations of $R(\mathbf{x}; 0, \tau)$ will not be forthcoming, owing to the nature of the numerical algorithm [21].

Our general form for R_{ij} , Eqn. (5.1), postdicts KH's data well and credibly predicts the cross correlations in turbulent boundary layer flow (Sec. V). In consequence we use (5.1) in Sec. VI to calculate a Lagrangian mean quantity which arises in mean field theory, the generalized Stokes drift. The results are discussed in Sec. VII.

II. BACKGROUND

A. The Kovasznay-Corrsin conjecture

We use as a starting point a notion due to Kovasznay [18] that the two-point two-time Eulerian correlation $Q_{ij}(\mathbf{x}; \mathbf{r}, \tau) = \langle u_i u_j \rangle R_{ij}(\mathbf{x}; \mathbf{r}, \tau) = \langle u_i(\mathbf{x}, t) u_j(\mathbf{x} + \mathbf{r}, t + \tau) \rangle$ can be expressed in terms of the diminution of the spatial product $u_i(\mathbf{x}, t) u_j(\mathbf{x} + \mathbf{r}, t)$. Here $u_i(\mathbf{x}, t)$ is the velocity of the flow at point \mathbf{x} at time t in an isotropic homogeneous turbulence and $\langle u_i \rangle$ denotes averaging over N repeated realizations; specifically

$$\langle u_i(t) \rangle = \lim_{N \rightarrow \infty} \frac{1}{N} \sum_{n=1}^N u_i^{(n)}(t).$$

In particular, Kovasznay reasoned that any diminution in the spatial product over time τ from its value at $\mathbf{r} = \mathbf{0}, \tau = 0$ is due to turbulent diffusion, vis a vis the fact that a fluid particle at $\mathbf{x} + \mathbf{r}$ at time τ , was at \mathbf{x} at $\tau = 0$. In terms of a generalized scalar function $\theta(\mathbf{x}, t)$ then

$$\begin{aligned} \langle u_i u_j \rangle R_{ij}(\mathbf{x}; \mathbf{r}, \tau) = \\ \int \langle u_i(\mathbf{x}, t) u_j(\mathbf{x} + \mathbf{p}, t) \theta(\mathbf{x} + \mathbf{p} - \mathbf{r}, t + \tau) \rangle d\mathbf{p}. \end{aligned} \quad (2.1)$$

Corrsin [19] further conjectured that at sufficiently large time the distribution of random displacements \mathbf{r} from \mathbf{x} , must become statistically independent of particular realizations of the velocity field. In essence, that the diffusion process is, after large time, effectively the same as a random walk process and that in random walks the local velocity has after many steps negligible correlation with the total displacement. Thus

$$\begin{aligned} \int \langle u_i(\mathbf{x}, t) u_j(\mathbf{x} + \mathbf{p}, t) \theta(\mathbf{x} + \mathbf{p} - \mathbf{r}, t + \tau) \rangle d\mathbf{p} \sim \\ \int \langle u_i(\mathbf{x}, t) u_j(\mathbf{x} + \mathbf{p}, t) \rangle \bar{\theta}(\mathbf{p} - \mathbf{r}, \tau) d\mathbf{p} \end{aligned}$$

where $\bar{\theta}(\mathbf{r}, \tau)$ is the probability that a fluid particle makes the displacement \mathbf{r} in time τ .

Of course what constitutes ‘large time’ is crucial to the usefulness of the conjecture, but that was quantified by Roberts [22] who, on the basis of an analysis by Kraichnan [23], determined statistical independence to be a reasonable approximation for times short enough such that $R_{ij}(\mathbf{x}; \mathbf{r}, \tau)$ is an appreciable fraction of unity. With that in mind, Saffman [24] utilized the conjecture to relate Lagrangian to Eulerian correlations in stationary homogeneous turbulence.

In the present context the conjecture says

$$R_{ij}(\mathbf{x}; \mathbf{r}, \tau) \approx \int_{-\infty}^{\infty} R_{ij}(\mathbf{x}; \mathbf{p}, 0) \bar{\theta}(\mathbf{p} - \mathbf{r}, \tau) d\mathbf{p}, \quad (2.2)$$

from which it follows that evaluation of $R_{ij}(\mathbf{x}; \mathbf{r}, \tau)$ rests upon knowledge of $\bar{\theta}(\mathbf{x} - \mathbf{r}, \tau)$ and $R_{ij}(\mathbf{x}; \mathbf{r}, 0)$, to which we now turn attention.

B. An isotropic model

To proceed we introduce a rectangular cartesian coordinate system $\mathbf{x} = (x_1, x_2, x_3)$ with unit vectors $(\mathbf{i}, \mathbf{j}, \mathbf{k})$; orient x_1 in the streamwise direction and set $\mathbf{r} = (X_1, X_2, X_3)$. Then for a homogeneous turbulence advecting in the x_1 direction at a constant mean convection velocity $V_j = (V, 0, 0)$, we have [18]

$$(2\pi)^{\frac{3}{2}} (\langle y_1^2 \rangle \langle y_2^2 \rangle \langle y_3^2 \rangle)^{\frac{1}{2}} \bar{\theta}(\mathbf{x} - \mathbf{r}, \tau) = \exp\left[-\frac{1}{2} \left\{ \frac{(X_1 - x_1 - V\tau)^2}{\langle y_1^2 \rangle} + \frac{(X_2 - x_2)^2}{\langle y_2^2 \rangle} + \frac{(X_3 - x_3)^2}{\langle y_3^2 \rangle} \right\}\right], \quad (2.3)$$

where $\langle y_i^2 \rangle$ is the mean square displacement of a marked particle in time τ .

We know also that the correlation for an isotropic turbulence, $R_{ij}(\mathbf{r}, 0) (\equiv R_{ij}(\mathbf{x}; \mathbf{r}, 0))$, can be expressed in terms of the longitudinal $\langle u_1^2 \rangle f(s) = \langle u_1(\mathbf{0}, t) u_1(\mathbf{i}s, t) \rangle$ and transverse $\langle u_1^2 \rangle g(s) = \langle u_2(\mathbf{0}, t) u_2(\mathbf{i}s, t) \rangle$ velocity correlations through [25]

$$R_{ij}(\mathbf{s}, 0) = \frac{f(s) - g(s)}{s^2} x_i x_j + g(s) \delta_{ij}, \quad (2.4)$$

where $s^2 = x_1 x_1 + x_2 x_2 + x_3 x_3$, and from continuity

$$f(s) + \frac{s}{2} \frac{\partial f}{\partial s} = g(s) \quad (2.5)$$

with $f(0) = 1$. But to go further requires $f(s)$.

At this point we appeal to experiment where there is strong evidence that $f(s)$ is gaussian, or nearly [26], so we let

$$f(s) = \exp\left[-\frac{1}{2} \left(\frac{s}{L}\right)^2\right]. \quad (2.6)$$

Here L is an appropriate length scale (which, with no loss of generality, we assume is component dependent and write as L_j).

Then with (2.3) and (2.6), (2.2) becomes [17],

$$R_{11}(\mathbf{r}, \tau) = \frac{e^{-N^2/2}}{D^3}. \quad (2.7)$$

Here $N^2 = N_1^2 + N_2^2 + N_3^2$ and

$$N_j^2 = \frac{(X_j - V_j \tau)^2}{L_j^2(1 + \frac{\langle y_j^2 \rangle}{L_j^2})} \quad (j = 1, 2, 3), \quad (2.8)$$

while $D^3 = D_1 D_2 D_3$ where

$$D_j = (1 + \frac{\langle y_j^2 \rangle}{L_j^2})^{\frac{1}{2}}. \quad (2.9)$$

It is now a straightforward extension to deduce R_{ii} , ($i = 2, 3$) for which

$$R_{ii}(\mathbf{r}, \tau) = \frac{e^{-N^2/2}}{D^3} (1 - \frac{1}{2} B) \quad (i = 2, 3) \quad (2.10)$$

where $B = B_1 + B_2 + B_3$ and

$$B_j = \frac{1}{1 + \frac{\langle y_j^2 \rangle}{L_j^2}} \left[\frac{\langle y_j^2 \rangle}{L_j^2} + \frac{(X_j - V_j \tau)^2}{L_j^2(1 + \frac{\langle y_j^2 \rangle}{L_j^2})} \right] \quad (j = 1, 2, 3). \quad (2.11)$$

Finally we combine (2.7) and (2.10) to yield, for an isotropic homogeneous flow,

$$R_{ii}(\mathbf{r}, \tau) = \frac{e^{-N^2/2}}{D^3} [1 - \frac{1}{2} \Delta_{ii} B] \quad (i = 1, 2, 3), \quad (2.12)$$

where $\Delta_{ii} = \delta_{i2} + \delta_{i3}$. Observe that (2.12) recovers $f(s)$ and $g(s)$ as it should when $\tau = 0$.

C. Experimental support

Experimental support for (2.7) came from Favre [17], who obtained satisfactory agreement between measured values of $R_{11}(X_1, 0, 0, \tau)$ in homogeneous grid turbulence and (2.7) for times short with respect to the Lagrangian integral time scale. To complete the calculation he used the experimental value of L (later defined) and assumed $\langle y_i^2 \rangle$ quadratic in τ , which is in fact valid only for short time; it grows linearly in τ for large time [24]. In consequence his predictions at optimal delay, i.e. when $X_1 = V\tau$, decay as τ^{-3} rather than the asymptotically correct $\tau^{-\frac{3}{2}}$.

III. NONISOTROPIC TURBULENT SHEAR FLOW; CORRELATIONS AT OPTIMAL DELAY

Our intent here is to consider $R_{ij}(\mathbf{x}; \mathbf{r}, \tau)$ in inhomogeneous nonisotropic turbulent flows. We begin by noting that measured and computed space correlations in such flows at a given level in the direction of inhomogeneity z , bare strong resemblance to their counterparts in isotropic homogeneous turbulence. In consequence we explore the notion that (2.12) continues to apply in inhomogeneous flow, albeit with the assumption, since R_{ij} is now a function of z , that $R_{ij}(\mathbf{x}; \mathbf{r}, \tau) \mapsto R_{ij}(x_1, x_2, x_3 + z; \mathbf{r}, \tau) \equiv R_{ij}(z; \mathbf{r}, \tau)$ for $z \neq 0$, i.e. away from boundaries.

Accordingly L_i , $\langle y_i^2 \rangle$ and V are also z -dependent. The dependence of each is deduced in subsequent sections using turbulent channel flow as a guide, but first we require the variation of $\langle y_i^2 \rangle$ with time, and in particular the correlation at optimal delay.

A. The form of $\langle y^2 \rangle$ with τ .

$\langle y_i^2 \rangle$ is the second moment of $\bar{\theta}$ with respect to X_1 and has the physical interpretation given in Sec. IIA; our intent here is to determine its detailed variation with τ . To isolate that behavior we consider the correlation at fixed z at optimal delay, i.e. at the delay determined by the mean convection velocity. Then $X_1 = V\tau$ and, with $X_2 = X_3 = 0$, the numerator in (2.12) is unity.

Details of $R_{ii}(z^+; V^+\tau^+, 0, 0, \tau^+)$ for $i = 1, 2, 3$ at $z^+ = 12$ follow from the contour plots in Fig. 13 of KH1 and are replotted in Fig. 1 with the displacement from the peak $X_1^+ = V^+\tau^+$ as the independent variable.

In order to isolate $\langle y_i^2 \rangle$, however, we require L_i and thus define L_i as the value of X_{1i} at which $R_{ii}(V\tau, 0, 0, \tau; z) = 1/2$. Then for each i

$$\eta = \frac{X_{1i}}{L_i} = \frac{V\tau_i}{L_i} \quad (3.1)$$

causing the data for R_{ii} , when plotted with η as the independent variable, to collapse at $\eta = 1$.

When plotted in this manner, however, the data for all three cases collapse not only at $\eta = 1$, but over the whole range of η ; see Fig. 2. This indicates that the functional form for the time evolution of $\langle y_i^2 \rangle / L_i^2$ has little if any dependence on direction, allowing us to write $\langle y_i^2 \rangle / L_i^2 = \mathcal{F}(\eta)$.

But does the function $\mathcal{F}(\eta)$ depict the same asymptotic behavior with τ as its homogeneous isotropic counterpart? There, $\langle y_i^2 \rangle$ is quadratic in τ for time small compared with the Lagrangian time scale and linear in τ for larger time. To resolve this question (2.12) was evaluated for each asymptotic form. Both asymptotes concur well with the data, as we see in Fig. 2, although agreement at small η is to some degree forced.

Nevertheless we have sufficient justification to craft an asymptotically correct form for $\mathcal{F}(\eta)$ and thus write

$$\mathcal{F}(\eta) = \frac{\eta^2}{(1 + A\eta^n)^{\frac{1}{n}}}. \quad (3.2)$$

Here n is a positive constant and, to ensure $R_{ii}(\eta, \tau; z) = 1/2$ at $\eta = 1$, set the constant $A = \gamma^n - 1$ with $\gamma \approx 1.7024$. Eq. (2.7), utilizing (3.2) with $n = 2$ (which together lead to Eq. (3.4)), is also plotted in Fig. 2 and is seen to provide a credible fit to the data.

Now the ubiquity - by which we mean the removal of effects due to inhomogeneity and nonisotropy - implied by (3.2) and (3.4) is intriguing and warrants investigation. To gain insight into it, recall that in the absence of a convection velocity $\langle y_i^2 \rangle$ varies as $\langle u_i^2(z) \rangle$ for all τ [24], so that for consistency in the presence of shear it is appropriate to replace V in (3.1) with, say $V + \langle u_i^2(z) \rangle^{\frac{1}{2}}$. Then in view of (3.2) we have

$$\frac{\langle y_i^2 \rangle}{L_i^2} = \frac{(V + \langle u_i^2(z) \rangle^{\frac{1}{2}})^2 \tau^2}{L_i^2 [1 + (\frac{\tau}{T_i})^n]^{\frac{1}{n}}}, \quad (3.3)$$

where T_i is the Lagrangian time scale. Observe that (3.3) concurs with Saffman [24] for $V^2 \ll \langle u_i^2(z) \rangle$ while $\langle y_i^2 \rangle / L_i^2 \sim \mathcal{F}(\eta)$ for $V^2 \gg \langle u_i^2(z) \rangle$. In short, the form $\mathcal{F}(\eta)$ is a consequence of advection rather than a profound anomaly due to turbulent diffusion.

In consequence we postulate that (3.2) is ubiquitous to any shear flow in which $V^2 \gg \langle u_i^2(z) \rangle$, from which it follows that the ubiquitous correlation coefficient at optimal delay, $\mathcal{R}(\eta)$, is independent of z and i , and has the form

$$\mathcal{R}(\eta) = (1 + \mathcal{F}(\eta))^{-\frac{3}{2}}. \quad (3.4)$$

Of course both $\langle y_i^2 \rangle$ and L_i^2 remain functions of z ; (3.4) simply means they each exhibit the same dependency with z .

B. A model for nonhomogeneous flow

The unfolded version of (3.4) is

$$R_{ii}(z; V\tau, 0, 0, \tau) = D_i^{-3} \quad (3.5)$$

which, necessitates D in (2.12) be replaced with D_i ; it also requires $B \ll 1$, at least for $X_1 = V\tau$. Eqn. (3.5) recovers the original data well, as we see in Fig. 1., albeit with known values of L_i . To be useful, however, it is necessary to ascertain the value of L_i for each i and its variation with z , and we shall do so in Secs IIIC and D.

C. The variation of L_i with z

To proceed we first need KH's values of L_i and these were deduced as follows: Each curve on KH2 Fig. 3 (which plots R_{ii} as a function of X_1^+ at various values of z^+ at fixed time delay τ^+) depicts the value of R_{ii} at $X_1 = V\tau$ and thus defines a point on the optimal delay curve \mathcal{R} . So, because \mathcal{R} is single valued in η , knowing \mathcal{R} defines η which in turn, through (3.1) defines L_i , which is plotted in Fig. 3. Observe that the half-width goes as $L_1^+ > L_2^+ \geq L_3^+$, in accord with the turbulence intensities.

Of course the next step is to construct an expression for L_i and we do so in Sec. IIID via an expression for the Lagrangian time scale, which we now discuss.

D. The Lagrangian time scale

In writing (3.3) we introduced the Lagrangian time scale T_i ; this may be estimated by comparing (3.3) with (3.2) to yield

$$T_i(z) = \frac{VL_i}{\gamma(V^2 + \langle u_i^2 \rangle)}. \quad (3.6)$$

Alternatively we may derive T_i from (3.4) (by noting that the long time asymptote is valid at $\eta \approx 1$ (see Fig. 2) and that L_i is defined in terms of $\langle y_i^2 \rangle$ when $\eta = 1$, so $L_i^2 = \gamma \langle y_i^2 \rangle|_{\eta=1}$).

KH's data for T_i (as determined from (3.6)) are plotted in Fig. (4), where we see that T_i^+ increases monotonically with z^+ in the outer region, although less rapidly than L_i^+ . Our task is to find a simple fit for T_i .

In order to do so we first normalize T_i by its centerline (i.e. maximum) value and plot the result in Fig. 5. Observe that the data for $i = 1, 2, 3$ more or less collapse in the outer region of the layer, while those in the inner region remain distinct. Such features are characteristic of bounded shear flows and are indicative of two categories of turbulent motions: those that actively contribute to the Reynolds stress and those that do not.

Townsend [35] denotes the former motions 'active' and the latter 'inactive'. Accordingly he associates the active component with smaller scale inner region motions and the inactive component with larger scale outer region motions, a notion supported by experiment [36].

The disparity in scales also permits their effects to be summed [27] and we exploit that point here. Specifically we assume T_i to be composed of an active and an inactive part.

Looking first at the outer region it is evident in Fig. 5 that $T_i/T_{i\infty}$ grows much like $(V/U_\infty)^m$ (see Fig. 6), where $2 < m < 3$, so we take this dependency to be the inactive component. Unfortunately details of the active component are less clear.

Previous studies [27] suggest that the active components of $\langle u_i^{+2}(z) \rangle$ are limited to values of $z^+ < P^+$, where $P^+ \approx 70$ is the characteristic thickness (in wall units) of the wall region [28]. But whether the active portions of $\langle u_i^{+2}(z) \rangle$, and by implication T_i^+ , are affected by Reynolds number is unclear: Indeed, the results of [20], [27] (see Fig. 5) and [29] suggest

little Reynolds number influence, while the results of [30], [31], [32], [33] suggest otherwise, particularly with regard to the intensity component normal to the wall.

Beyond that and KH's data at two values of z , we know no more. All we can surmise is that the form of T_i in the inner region is roughly that as sketched in Fig. 5, where we have assumed the active component goes like $ze^{-(z-z_0)^2}$, with z_0 constant. Thus,

$$\frac{T_i}{T_{i\infty}} = \left(\frac{V}{U_\infty}\right)^m + \alpha_i \frac{z}{z_\infty} e^{-(\frac{z-z_0}{\beta z_\infty})^2}. \quad (3.7)$$

In plotting Figs. 3, 4 and 5 we set $m = 5/2$, $\alpha_i = (8.5, 9.9, 2.0)$, $\beta = 20$ and $z_0/z_\infty = 1$. Equation (3.7) unfolds reasonably well to depict T_i , as we see in Fig. 4, as does L_i from (3.6) in Fig. 3. But until more data for the inner region are available, the form of the active component must be treated as speculative.

E. The convection velocity

In order to calculate (3.6) and (3.7) we also require knowledge of $\langle u_i^2 \rangle$ and V . Both of course are given by KH, but for more general calculations, it is useful to have an approximate expression for each. Asymptotically correct approximate expressions for $\langle u_i u_j \rangle$ and the Eulerian mean velocity U are given by Phillips & Ratnanather [27,34] while consistent expressions that link U_τ/U_∞ etc. with various Reynolds numbers (e.g. Re_θ , Re_δ^* , Re_τ) are given in [28]. Here we require an approximate expression for the convection velocity V .

KH find the propagation velocities of the three perturbation velocities are within a few percent of one another. In particular they find V depicts a lower bound in the wall region of about 0.55 % of the centerline velocity U_∞ and asymptotes to U_∞ in the outer region. For our present purposes we shall not distinguish between components; rather we construct a generic form for V from U . Specifically, since $U \sim z$ as $z \rightarrow 0$ and $dU/dz \rightarrow 0$ as $z \rightarrow z_\infty$ we write

$$V = AU_\infty \frac{U'}{U'(0)} + \frac{z}{z_\infty} \left(\frac{z_\infty + z_1}{z + z_1} \right) U. \quad (3.8)$$

Comparison with KH's curve for V^+ suggests that $A = 0.55$ and that z_1^+ lies in the range $5 - 10$. This curve concurs well with that of KH and is plotted in Fig. 6 with $z_1^+ = 7$.

Finally (3.8) should also carry over to boundary layers, where we interpret U_∞ and z_∞ as values at the characteristic thickness δ of the layer (see [34]).

IV. NONISOTROPIC TURBULENT SHEAR FLOWS; SPACE TIME CORRELATIONS

A. A general model for nonhomogeneous, nonisotropic flow

We turn attention now to correlations for which $X_1 \neq V\tau$ so that the numerator in (2.12) is non-zero. In fact rather than using (2.12) we introduce a more general form written as

$$R_{ii}(z; \mathbf{r}, \tau) = \frac{e^{-N_i^{*2}/2}}{D_i^3} \left[1 - \frac{1}{2} \Delta_{ii} B_i^* \right] \quad (i = 1, 2, 3). \quad (4.1)$$

Here B_i^* and N_i^* contain the same ingredients as B and N , but for generality may deviate in detailed form. For example, because the numerator must now depend on direction (which N does not) and because we expect R_{ii} to be z -dependent, we introduce the function $h_i(z)$ and write $N_i^{*2} = 2h_i^2 N^2$. Of course $2h_i^2 = 1$ in an isotropic, homogeneous flow, but will differ from unity otherwise. We discuss $h_i(z)$ in Sec. IV B and B_i^* in Sec. IV C.

First, however, we note that in order to evaluate B and N (or their modeled counterparts B_i^* and N_i^*) from KH's data we require $X_1 - V\tau$, L_i and $\langle y_i^2 \rangle / L_i^2$. The first is extracted directly from KH2 Fig. 3, while the second is known via η from Sec. IIIC. The third also follows from η using (3.2).

B. The function h_i and its variation with z

With N and N_i^* at hand we seek $h_i(z)$. Of course in general $N_i^{*2} = 2h_i^2(N_1^2 + N_2^2 + N_3^2)$

or

$$\frac{N_i^{*2}}{2} = \frac{h_i^2(X_j - V_j\tau)^2}{L_j^2(1 + \frac{\langle y_j^2 \rangle}{L_j^2})} \quad (\text{sum } j), \quad (4.2)$$

where we define $h_i(z)$ to ensure the half width, i.e. the spacing $|X_1 - V\tau|$ where $R_{ii}(\mathbf{r}, \tau) = D_i^{-3}/2$, is correctly predicted. So, setting $B_i^* = B_{iH}^*$, $N_i^* = N_{iH}^*$ and $N = N_H$ at the half point, then from (4.1),

$$N_{iH}^{*2} = 2h_i^2 N_H^2 = 2 \ln\{2[1 - \frac{1}{2}\Delta_{ii}B_{iH}^*]\}, \quad (4.3)$$

from which we extract $h_i(z)$.

KH give the necessary data to solve (4.3) at only four z -locations; nevertheless it is clear (see Fig. 7) that $h_1(z)$ is essentially linear. In fact

$$h_1(z) \approx 9 \frac{z}{z_\infty} + 1.5; \quad (4.4)$$

furthermore, h_2 and h_3 are about 80% higher than h_1 (they are scaled accordingly in Fig. 7) and so for modeling purposes we write $h_i = 1.8h_1$ ($i = 2, 3$).

C. The function B^*

The principal role of B or B_i^* is to render R_{22} and R_{33} negative for some values of $|X_1 - V\tau|$, which may vary with z (see KH2 Fig. 3). Of course the correlation can be negative only if $B^* > 2$ and that is not always achieved: as noted earlier, comparison of (3.5) with (4.1) at optimal delay necessitates $B^* \ll 1$.

In modeling B_i^* then, we must capture a z dependence tempered by $|X_1 - V\tau|$. Since $h_i(z)$ is known, the former may be realized by writing $B_i^* = 2h_i^2 B$, as we did with N_i^* . But there is an immediate problem, because (from (2.11)) $B \sim \langle y_i^2 \rangle / L_i^2 = O(1)$ at optimal delay, while the data require $\langle y_i^2 \rangle / L_i^2 \ll 1$. The reason for the disparity is that $\langle y_i^2 \rangle / L_i^2$ (as evaluated from (3.2)) is dominated by $V\tau$, whereas the portion of $\langle y_i^2 \rangle$ relevant to B_i^* is that relative to the convected component, i.e. $\langle u_i^2 \rangle \tau^2$. Thus rather than (2.11), we choose the form

$$B_i^* = \frac{h_i^2}{1 + \frac{\langle y_j^2 \rangle}{L_j^2}} \left[\frac{\langle u_j^2 \rangle \tau^2}{L_j^2} + \frac{(X_j - V_j \tau)^2}{L_j^2 (1 + \frac{\langle y_j^2 \rangle}{L_j^2})} \right] \quad (\text{sum } j) \quad (4.5)$$

where the label i refers to R_{ii} . Here B_i^* is z -dependent and exceeds two for some X_1 ; accordingly $B^* \ll 1$ at optimal delay.

Of course a crucial test is to compare (4.1) using (4.2), (4.4) and (4.5) with KH2 (Fig. 3). This we do in Fig. 8. Observe that the peak value of the correlation compares well at each z^+ , as does its X_1^+ location; the half widths are also credibly predicted. Of course if the peak values are correct then the curves at optimal delay must also be correct and are, as we saw in Fig. 1.

But not everything is perfect: the tails of the correlations in Fig. 8 decay much faster with $|X_1^+ - V^+ \tau^+|$ than do the DNS results. This is an effect due to Reynolds number (see Sec. IV D): in essence (4.1) describes the correlation as it occurs at infinite Reynolds number.

D. The influence of Reynolds number

To understand why the curves in Fig. 8 have different tails than their counterparts in KH we return to (2.3), which gives the probability that a fluid particle at $\mathbf{x} + \mathbf{r}$ at time τ was at \mathbf{x} at $\tau = 0$. The assumption in (2.3) was that the probability is gaussian, while the inference from KH's data is that the probability distribution gradually loses gaussianity as \mathbf{r} and τ increase, and eventually becomes independent of displacement and time.

The reason is as follows: (2.3) assumes the fluid is advecting in an unbounded domain. Specifically, that all particles arriving at a point at time τ lay somewhere within a conical volume at time $\tau = 0$. At finite Reynolds numbers, on the other hand, and for sufficiently large τ , the diameter of the cone must at some point exceed the spacing of the channel walls, causing (2.3) to break down. Indeed, at that stage, the source of particles arriving at the apex is restricted to an area bounded by the channel walls and there is then an even probability they came from any location within that area. The same argument applies to \mathbf{r} .

Thus, rather than employing (2.3), which has the form $e^{-\frac{1}{2}\kappa^2}$, the probability must take the more general form $e^{-\frac{1}{2}\text{erf}(\kappa^2)}$.

Of course $\text{erf}(\kappa^2) \sim \kappa^2$ for $\kappa^2 < 0.6$ and so the correlation is unaffected near its peak. Deviations elsewhere, however, and in particular in the tail of the correlation, are determined by the value of $X_1 - V\tau$ at which $\kappa^2 = 0.6$, and this concurrence is Reynolds number dependent. In consequence (4.1) is the limiting case of the correlation as it occurs at infinite Reynolds number.

V. CROSS CORRELATIONS

Equation (4.1) can be further generalized to R_{ij} ($i, j = 1, 2, 3$), as

$$R_{ij}(z; \mathbf{r}, \tau) = \frac{e^{-N_i^* N_j^*/2}}{(D_i D_j)^{\frac{3}{2}}} \left[1 - \frac{1}{4} (\Delta_{ii} + \Delta_{jj}) (B_i^* B_j^*)^{\frac{1}{2}} \right], \quad (5.1)$$

which accounts for cross correlations. KH do not present cross correlations but Favre [17] (Fig. 12) does. In particular he plots $R_{13}(z; X_1, 0, X_3, \tau)$ in a boundary layer, with z set to 13.5% of the boundary layer thickness and $X_1 = U\tau$. The Reynolds number of his boundary layer ($Re_\delta = 31,200$, based on free stream velocity and δ) far exceeds that of KH's channel flow ($Re_h = 3260$ based on free stream velocity and channel half width). Nevertheless on setting z to 13.5% of the channel half width, we see (in Fig. 9a) that the model depicts the same features as the boundary layer data (Fig. 9c) but with a lower decay rate both in X_1 and X_3 . This of course could highlight a deficiency with the model, but it is more likely a Reynolds number effect.

To gain insight into the effect of Reynolds number, we plot a third case (Fig. 9b). Since Favre gives scant details of his flow, we use [27], [28] and [34] to instead simulate U^+ and $\langle u_i^+ u_j^+ \rangle^{\frac{1}{2}}$ in Purtell *et al*'s [37] boundary layer at an $Re_\theta = 1840$ ($Re_\delta \approx 17000$), shown in figure 10. At this Reynolds number the model predicts a slower decay in X_1 for $X_1/\delta < 1/2$ but more or less concurs with Favre's data for $X_1/\delta > 1/2$. The decay in X_3 on the other hand is faster than Favre's data, but not greatly. In any event Fig. 9b is a fair *prediction*

of Fig. 9a, as opposed to the *postdiction* of Fig. 8 and suggests that our expression for L_i carries over to boundary layers.

VI. AN EXAMPLE

With a model of R_{ij} to hand, it is appropriate to now recall our motivation for constructing it, viz a vis its use in techniques to deduce turbulence structure, and employ it in an example. We do so in the context of Lagrangian mean field theory applied to parallel shear flows as outlined in [8], where the theory is used to describe the dynamics (birth, death and rebirth) of streaks and longitudinal vortices.

Of course like their Eulerian averaged counterparts, Lagrangian averaged equations are not closed; the former requiring quantities like Q_{ij} , the latter quantities like the generalized Stokes drift. But while Q_{ij} can, for the most part, be measured by fixed instruments or calculated numerically in an Eulerian field direct simulation, Lagrangian mean quantities cannot. Fortunately, however, there are instances where Lagrangian mean quantities can be expressed in terms of Q_{ij} . One such instance is that of a discrete (or continuous) spectrum of three (or two) dimensional finite amplitude rotational waves on a parallel shear flow, as occur in KH's flow.

Phillips [10] analyses this case in detail and shows that the streamwise component of the generalized Stokes drift D_1 , which as $U + D_1$ is the mass transport velocity, takes the form

$$D_1(z, t) = \frac{\partial}{\partial z} \int_0^{\kappa^*} Q_{31}^* d\tau - \frac{U''}{2} \int_{\kappa^*}^0 \int_0^\zeta Q_{33}^* d\tau d\zeta. \quad (6.1)$$

Here Q_{ij}^* is the space-time correlation at optimal delay and κ^* is a value of τ at which R_{ij}^* satisfies specific constraints (see [10]). We evaluate (6.1) using (5.1) and KH's data for the Reynolds stress tensor, and plot the results as D_1^+ in Fig. 11. Here we see that mass transport is slower than the Eulerian mean flow in the wall region and exceeds it in the outer region. We further note that the peak deficit occurs at a z^+ value very close to that at which $\langle u_1^2 \rangle$ is a maximum.

VII. DISCUSSION

We have used the Kovasznay-Corrsin conjecture, supplemented by two auxiliary functions, to construct a generic form for space-time correlations in turbulent shear flows. The form is relatively simple and is useful to interpolate correlations intermediate to those measured or calculated. The auxiliary functions account for variations in the direction of inhomogeneity and were derived in detail for turbulent channel flow. Of course it is doubtful the precise functions deduced for channel flow will apply to all shear layers, although they seem appropriate for boundary layers.

In analyzing the channel flow data, it transpired that the correlations at optimal delay depict, when appropriately normalized, a form independent of turbulence component. This is not the case in homogeneous isotropic flows where, while R_{11} is strictly positive, R_{22} and R_{33} are not. Of course the present result is true only to leading order and over the range of X_1^+ for which the DNS statistics are credible. Nevertheless it is a useful approximation for the purposes of analysis up to spacings say of 1000 or so wall units.

Fluid particles arriving at a point in unbounded space are drawn from anywhere within a conical region that extends upstream of the point. In bounded flows, however, and at sufficiently large separations in space and/or time upstream of the point, the cone intersects the wall. The sourceable volume is thereby restricted and because details of the cone-wall interaction are affected by Reynolds number, the ensuing space-time correlation is Reynolds number dependent, most particularly in the tail of the correlation.

Of course we might expect that dependence to scale with wall variables in the wall region, but that need not be the case. Specifically, while wall variables are a useful first cut for scaling events normal to the wall, there is no immediate reason why such scaling should apply in the streamwise direction, although for consistency we write streamwise distance in such variables.

KH find R_{11} exceeds 0.1 throughout the shear layer until at least $X_1/\delta = 5$ (see Fig. 8), while (5.1) at infinite Reynolds number suggests zero correlation at the same separation.

Equation (5.1) can of course be configured to recover KH's observed tail (see Sec. IV D) but although nonzero correlations are conceivable in some regions of z in bounded shear layers at separations $X_1/\delta \gg 1$, it is doubtful they remain nonzero throughout the shear layer, particularly at geophysical Reynolds numbers.

Finally, as motivation for this work we cited the requirements of techniques designed to deduce the structure of turbulent flows. Interestingly, although each method cited employs R_{ij} , they each utilize a different form of R_{ij} . For example, proper orthogonal decomposition needs the correlation at zero time delay, while mean field theory requires it at close to optimal time delay. Linear stochastic estimation, on the other hand, can make use of the full space-time correlation, although calculations to this point have been restricted to zero time delay. Equation (5.1) vastly exceeds these requirements, but that may not be the case for the next generation of structure educing techniques, which we infer will also be built around space-time correlations.

In short (5.1) provides an ideal basis function from which to approximate R_{ij} in turbulent shear flows. It is rendered complete with the following equations: (3.6), (3.7) and (3.8), which define L_i , T_i and V and thus η from (3.1). Equation (3.2) then provides $\langle y_i^2 \rangle / L_i^2$ enabling the evaluation of D_i from (2.9), and N_i^* and B_i^* from (4.2), (4.4) and (4.5).

ACKNOWLEDGMENTS

The work was supported by the National Science Foundation through grants OCE-9696161 and OCE-9818092.

REFERENCES

- [1] A.A. Townsend, *The Structure of Turbulent Shear Flow* (Cambridge University Press, Cambridge , 1956).
- [2] J.L. Lumley, "Coherent structures in turbulence," in *Transition and Turbulence* edited by R.E. Meyer (Academic Press, New York , 1981).
- [3] P. Moin and R.D. Moser, "Characteristic eddy decomposition of turbulence in a channel," J. Fluid Mech. **200**, 471 (1989).
- [4] R.J. Adrian and P. Moin, "Stochastic estimation of organized turbulent structure: Homogeneous shear flow," J. Fluid Mech. **190**, 531 (1988).
- [5] W.R.C. Phillips, "The generalized Lagrangian mean equation: turbulent channel flow and streamwise vortices," in *Near wall turbulence* edited by S.J. Kline and N.H. Afgan (Hemisphere, Washington , 1989), p 736.
- [6] W.R.C. Phillips, "On the etiology of shear layer vortices," Theor. Comp. Fluid Dyn. **2**, 329 (1991).
- [7] S. Leibovich, "Structural genesis of wall bounded turbulent flows," in *Studies in Turbulence* edited by T. Gatski, S. Sarkar and G. Speziale (Springer, Berlin , 1992), p387.
- [8] W.R.C. Phillips, "On the nonlinear instability of strong wavy shear to longitudinal vortices," in *Nonlinear Instability, Chaos and Turbulence* edited by L. Debnath and D.N. Riahi (Comp. Mech. Publns, UK , 1998), p 277.
- [9] W.R.C. Phillips, "Finite amplitude rotational waves in viscous shear flows," Stud. Appl. Math **101**, 23 (1998).
- [10] W.R.C. Phillips, "On the pseudomomentum and generalized Stokes drift in a spectrum of rotational waves," J. Fluid Mech. (in revision) (2000).
- [11] A.J. Favre, J.J. Gaviglio R. and Dumas, "Space-time double correlations and spectra

- in a turbulent boundary layer,” J. Fluid Mech. **2**, 313 (1957).
- [12] S. Herzog, “The large scale structure of the near wall region of turbulent pipe flow,” Ph.D. thesis Cornell University, 1986.
 - [13] M.N. Glauser, S.J. Leib and W.K. George, “Coherent structure in the axisymmetric jet mixing layer,” in *Proc. 5th Symp of the Turbulent Shear Flow* (Springer, Berlin 1985).
 - [14] J. Kim and F. Hussain, “Propagation velocity and space-time correlations of perturbations in turbulent channel flow,” NASA TM-103932, 1992.
 - [15] J. Kim and F. Hussain, “Propagation velocity of perturbations in turbulent channel flow,” Phys. Fluids **5**, 695 (1993).
 - [16] J. Kim, P. Moin and R. Moser, “Turbulence statistics in fully developed channel flow at low Reynolds number,” J. Fluid Mech. **177**, 133 (1987).
 - [17] A.J. Favre, “Review of space time correlations in turbulent fluids,” J. Appl. Mech. **17**, 241 (1965).
 - [18] L.S.G. Kovasznay, Turbulence in supersonic flow J. Aeronaut. Sc. **20**, 657 (1953).
 - [19] S. Corrsin, “Proceedings of the Oxford Symposium on Atmospheric Diffusion and air pollution,” 162, (Academic Press, New York , 1960).
 - [20] R. Moser, J. Kim and N.N. Mansour, “Direct numerical simulation of turbulent channel flow up to $Re_\tau = 590$ ” Phys. Fluids **11** 943 (1999).
 - [21] R. Moser, private communication (1999)
 - [22] P.H. Roberts, J. Fluid Mech. “Analytical theory of turbulent diffusion,” **11**, 257 (1961).
 - [23] R.H. Kraichnan, “The structure of isotropic turbulence at very high Reynolds number,” J. Fluid Mech. **5**, 497 (1959).
 - [24] P.G. Saffman, “An approximate calculation of the Lagrangian auto-correlation coeffi-

cient for stationary homogeneous turbulence,” Appl. Sc. Res. **11**, 245 (1963).

- [25] J.O. Hinze, *Turbulence* McGraw Hill (McGraw Hill, New York , 1975).
- [26] G.K. Batchelor and A.A. Townsend, “Turbulent diffusion,” in *Surveys in Mechanics* (Cambridge University Press, Cambridge , 1956).
- [27] W.R.C. Phillips, “The wall region of a turbulent boundary layer,” Phys. Fluids **30**, 2354 (1987).
- [28] W.R.C. Phillips, “On the logarithmic law constants and the turbulent boundary layer at low Reynolds numbers,” Appl. Sc. Res. , **52**, 279 (1994).
- [29] L.P. Erm and P.N. Joubert, “Low-Reynolds number turbulent boundary layers,” J. Fluid Mech. **230**, 1 (1991).
- [30] T. Wei and W.W. Willmarth, “Reynolds-number effects on the structure of a turbulent channel flow,” J. Fluid Mech. **204**, 57 (1989).
- [31] J.C. Klewicki and R.E. Falco, “On accurately measuring statistics associated with small-scale structure in turbulent boundary layers using hot-wire probes,” J. Fluid Mech. **219**, 119 (1990).
- [32] R.A. Antonia, M. Teitel, J. Kim and L.W.B. Browne, “Low-Reynolds-number effects in a fully developed turbulent channel flow,” J. Fluid Mech. **236**, 579 (1992).
- [33] R.A. Antonia and J. Kim, “Low-Reynolds-number effects on near wall turbulence,” J. Fluid Mech. **276**, 61 (1994).
- [34] W.R.C. Phillips and J.T. Ratnanather, “The outer region of a turbulent boundary layer,” Phys. Fluids **2**, 427 (1990).
- [35] A.A. Townsend, “Equilibrium layers and wall turbulence” J. Fluid Mech. **11**, 97 (1961).
- [36] P. Bradshaw, “Inactive motion and pressure fluctuations in turbulent boundary layers”

J. Fluid Mech. **30**, 241 (1967).

- [37] L.P. Purtell, P.S. Klebanoff and F.T. Buckley, "Turbulent boundary layer at low Reynolds number" Phys. Fluids **24**, 802 (1981).

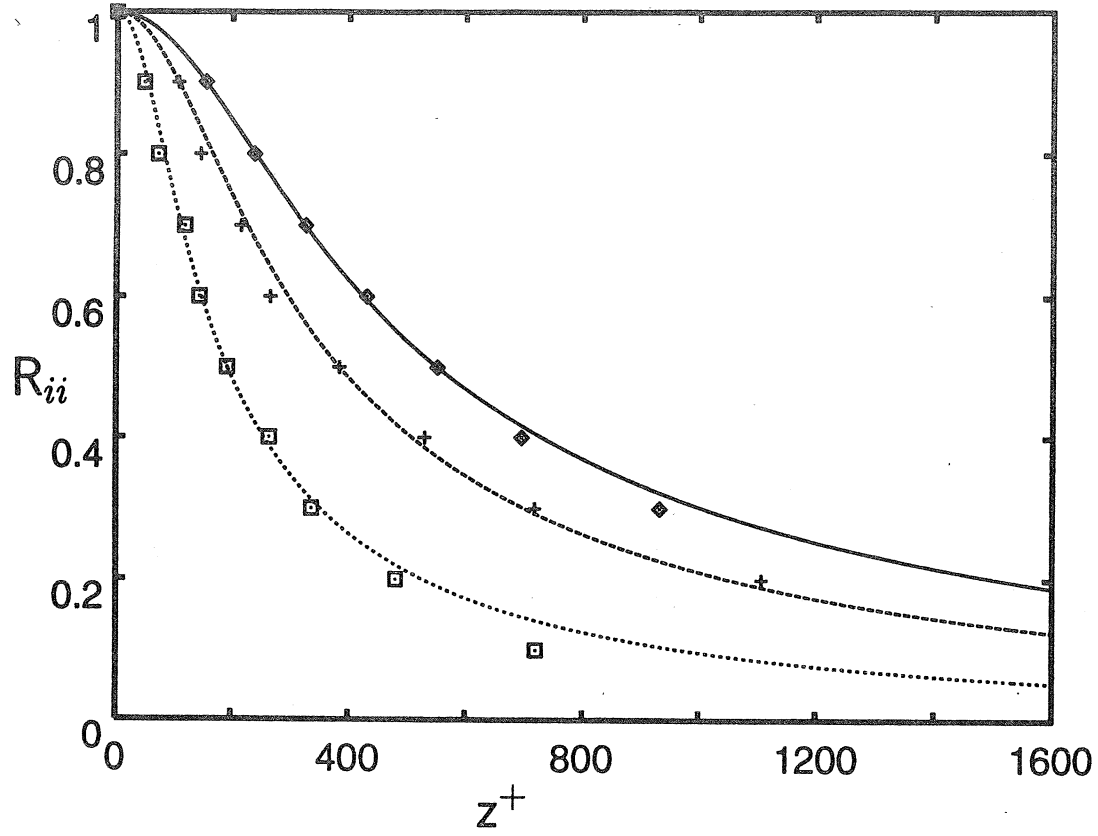


FIG. 1. Data of KH1 at $z^+ = 12$ for R_{ii} at optimal delay: \diamond Streamwise, $+$ transverse, \square wall normal. Curves from Eq (3.6) as recovered from (4.1)

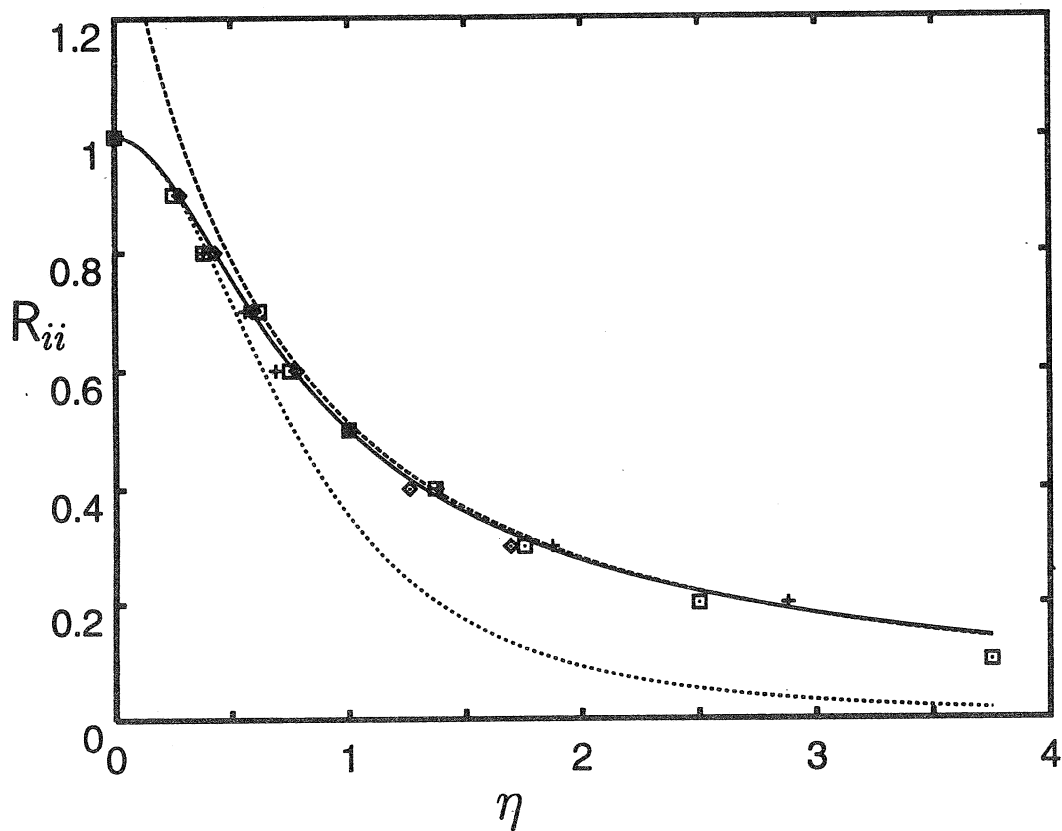


FIG. 2. Data of Fig.1 with independent variable normalized at $R_{ii} = 0.5$. Symbols as in Fig.1. The dashed lines are the asymptotic forms for small and large τ . Solid line Eq. (3.4).

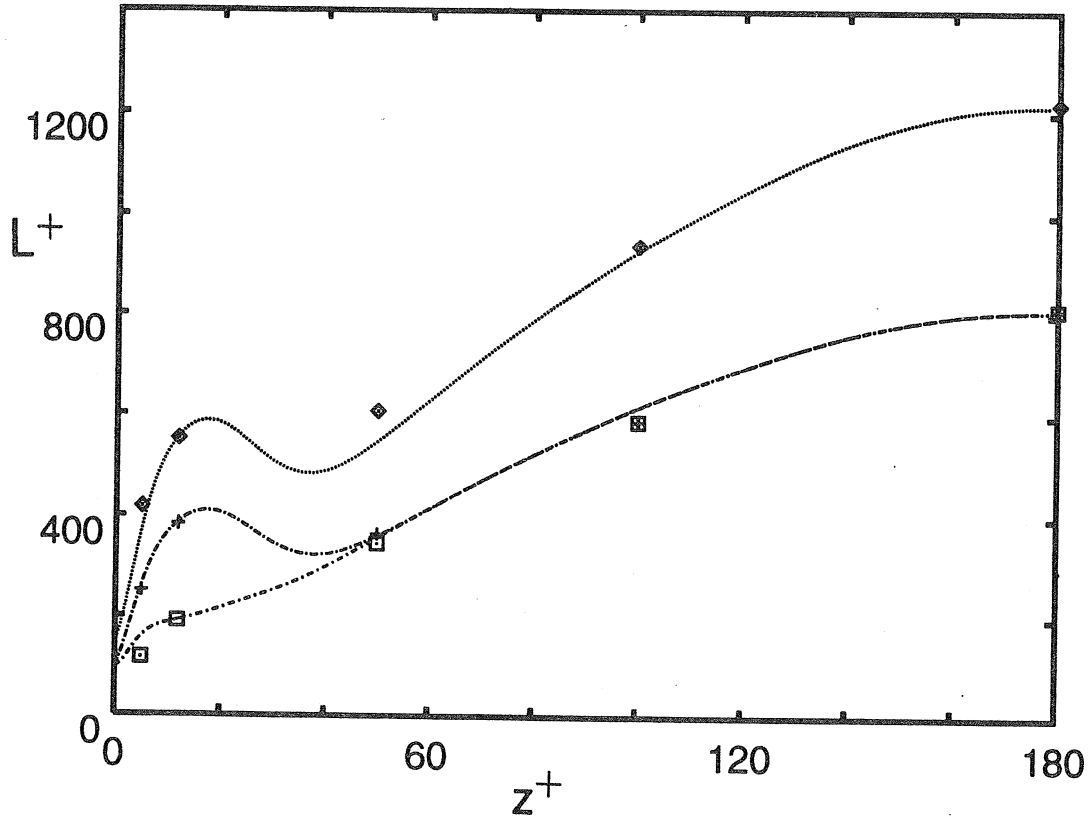


FIG. 3. The half width L_i as extracted from the data of KH. Symbols as in Fig. 1. Curves from Eq. (3.6) with $m = 2.5$.

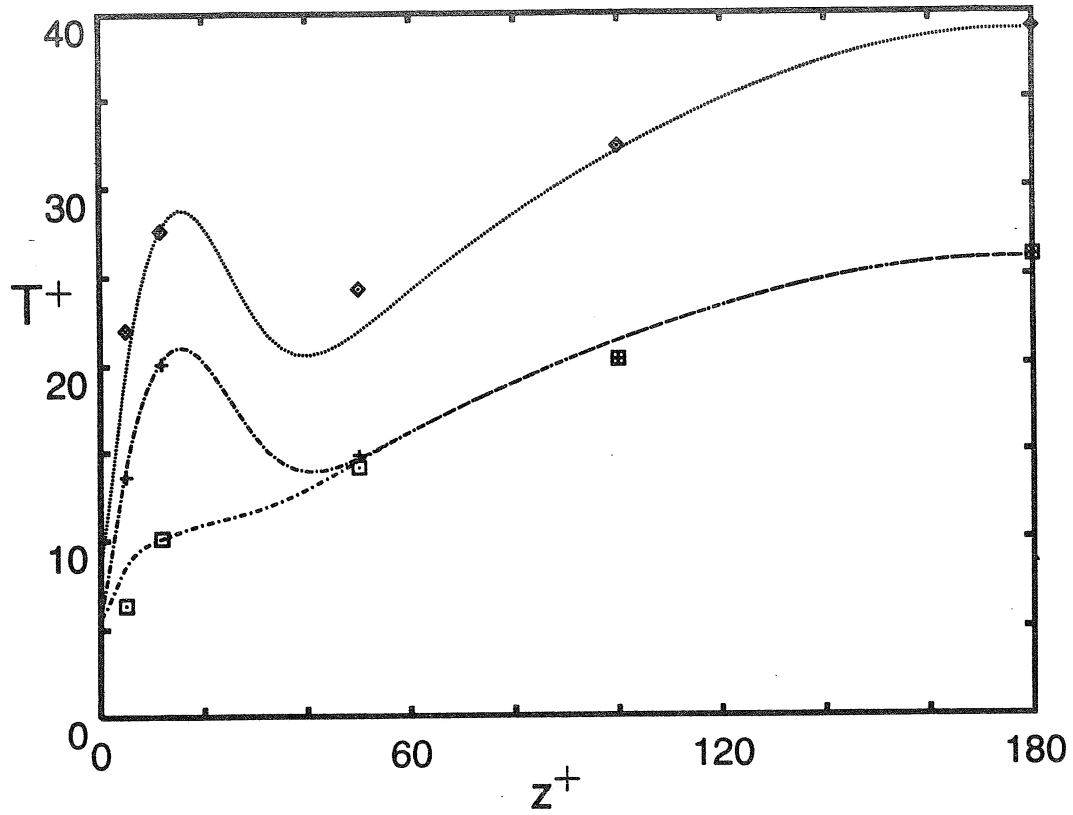


FIG. 4. The Lagrangian time scale T_i^+ as a function of z^+ as defined by Eq. (3.6). Symbols as in Fig. 1.

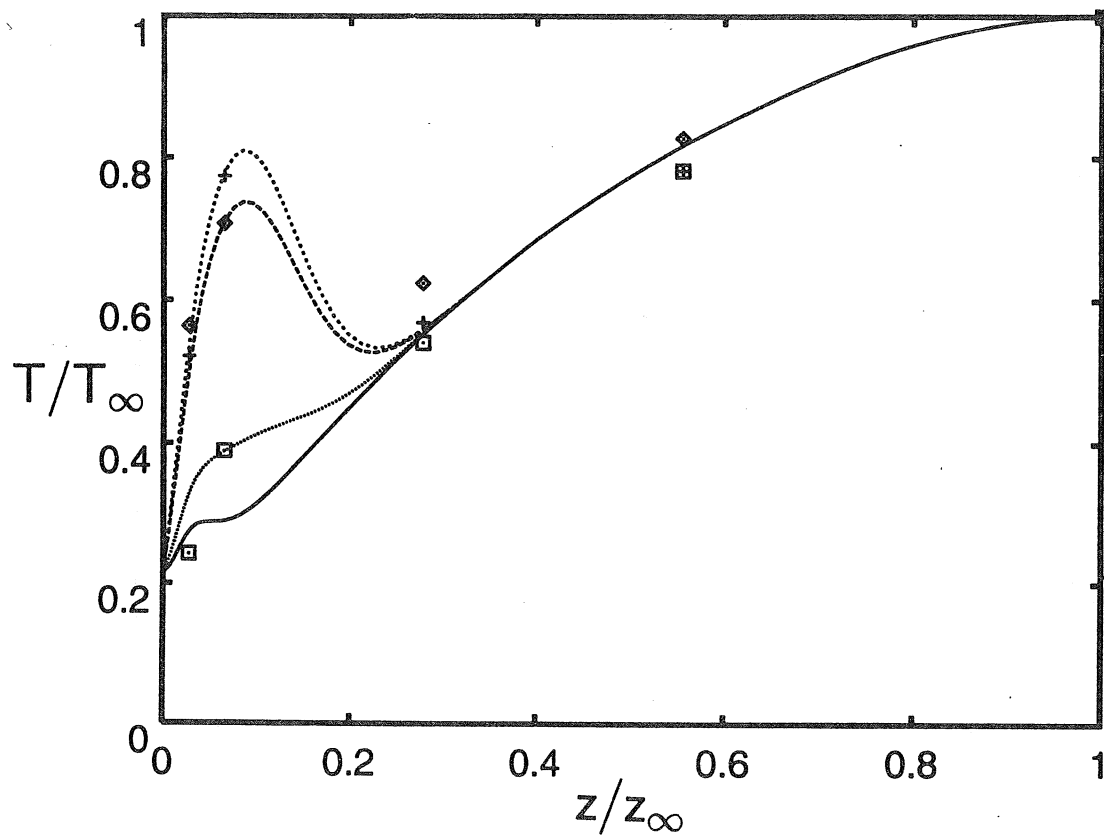


FIG. 5. Data from Fig. 4 normalized by centerline value. Symbols as in Fig. 1; $m = 2.5$.

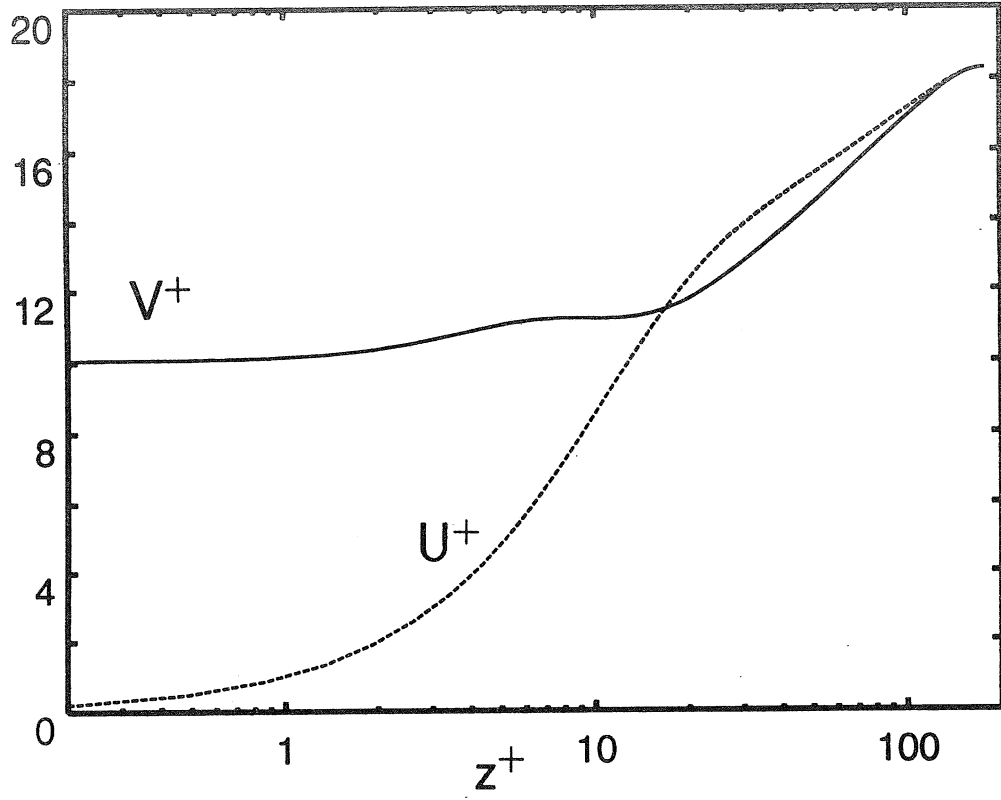


FIG. 6. Distributions of the convection velocity V^+ from Eq. (3.8) with $z_1^+ = 7$ and mean velocity U^+ from KH.

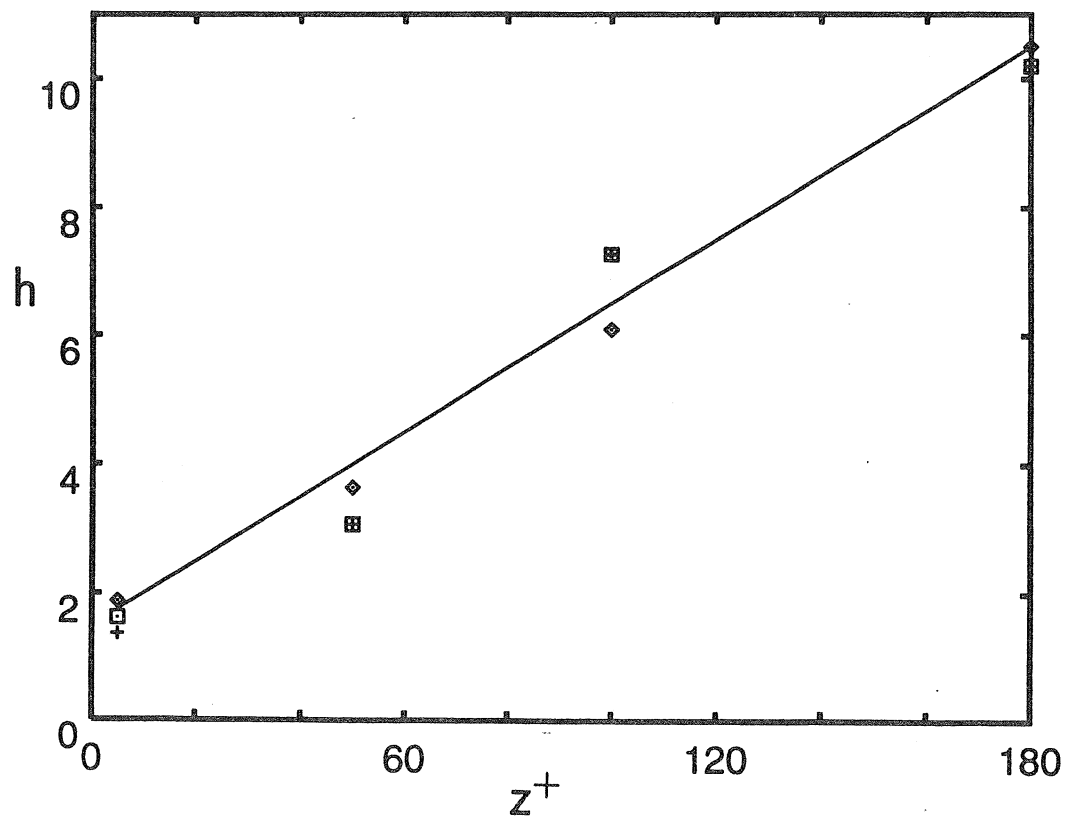


FIG. 7. Plot of the function h_i

FIGURE 8a, 8b

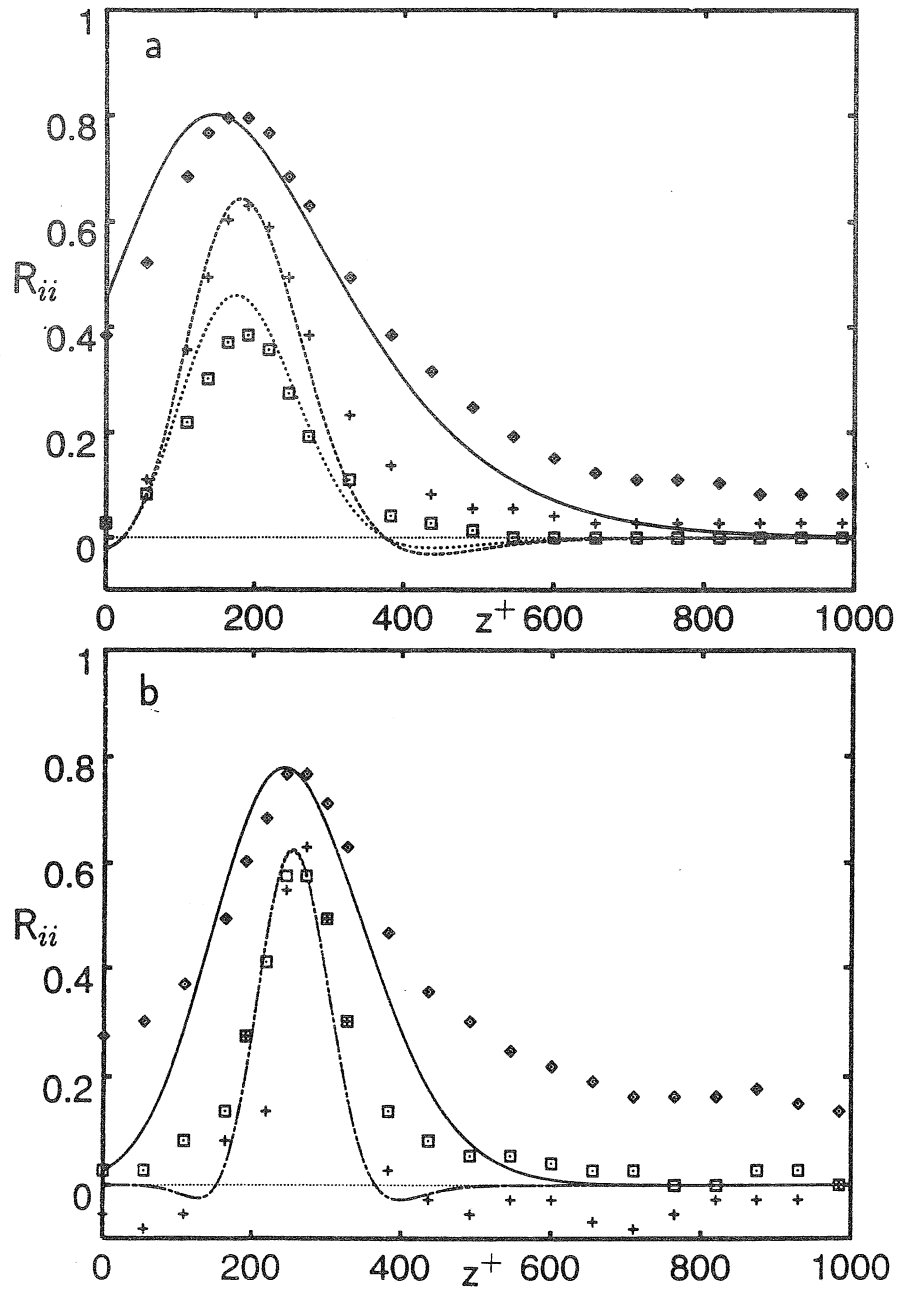
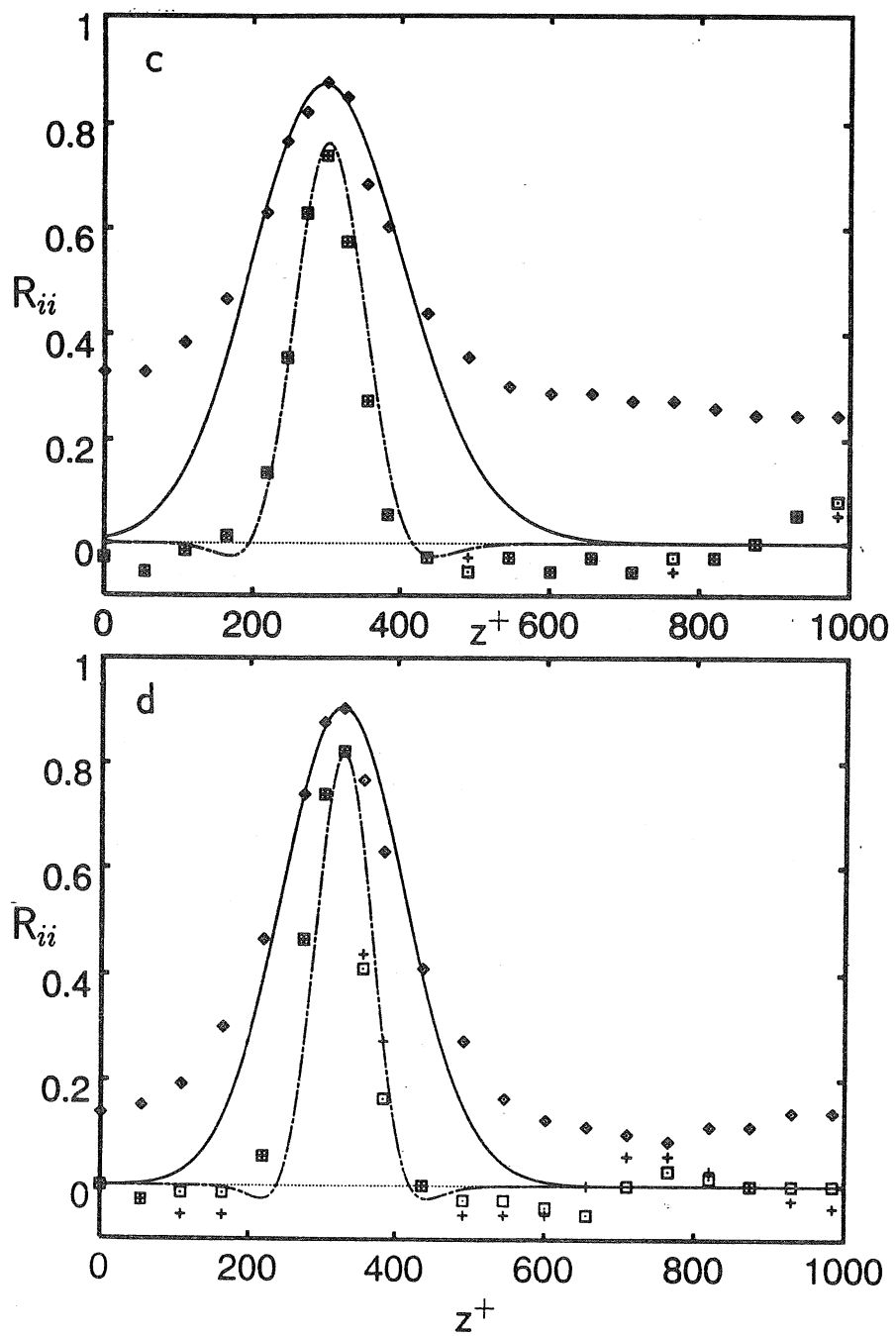


FIG. 8. Plots of R_{ii} from (4.1) at (a) $z^+ = 5$, (b) $z^+ = 50$, (c) $z^+ = 100$, (d) $z^+ = 180$. Data of KH2 Fig. 3: \diamond streamwise; $+$ transverse; \square wall normal.

FIGURE 8c, 8d



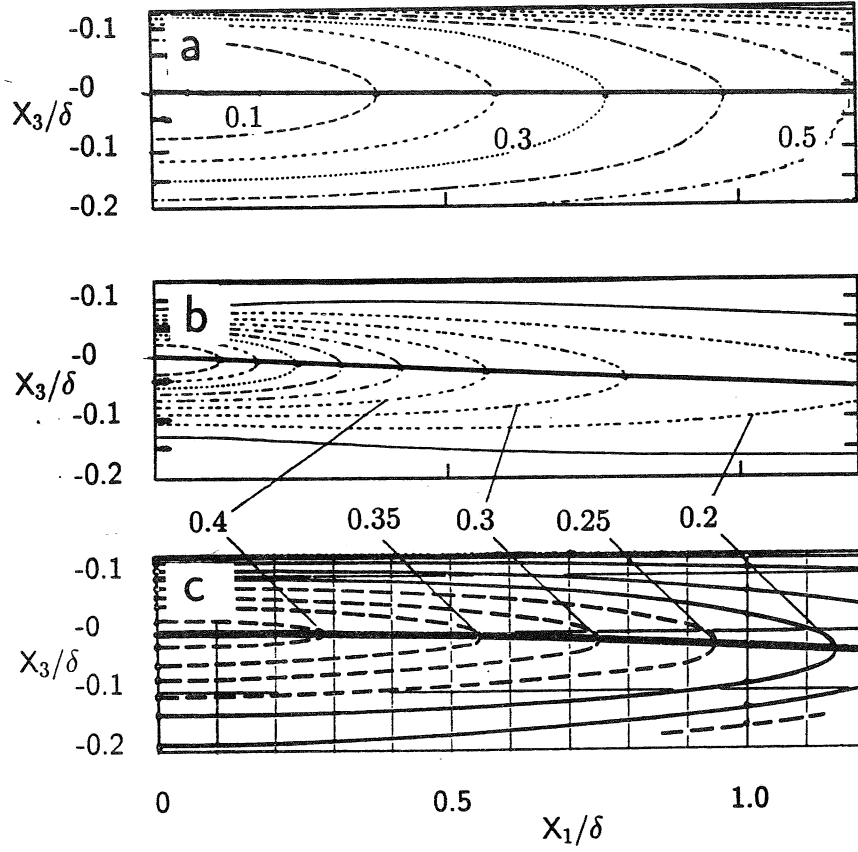


FIG. 9. Contours of R_{ij} at optimal delay at $z/\delta = 0.135$. (a), KH's channel flow, $Re_\delta = 3260$; (b), a modeled boundary layer at $Re_\theta = 1840$ ($Re_\delta \approx 17,000$); (c), data of Favre [17] in a boundary layer at $Re_\delta = 31,200$.

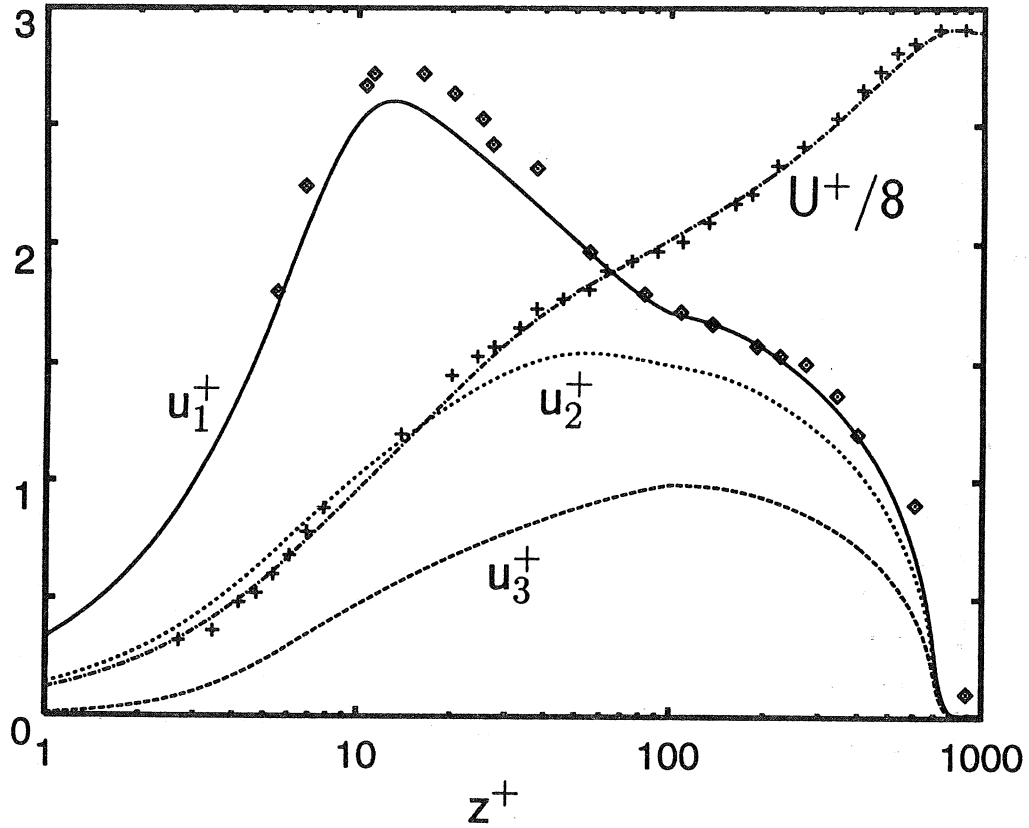


FIG. 10. Plots of U^+ and $\langle u_i^+ u_j^+ \rangle^{\frac{1}{2}}$ for $Re_\theta = 1840$ as calculated from [27,28,32]. Data of Purtell *et al* [35] at the same Re_θ .

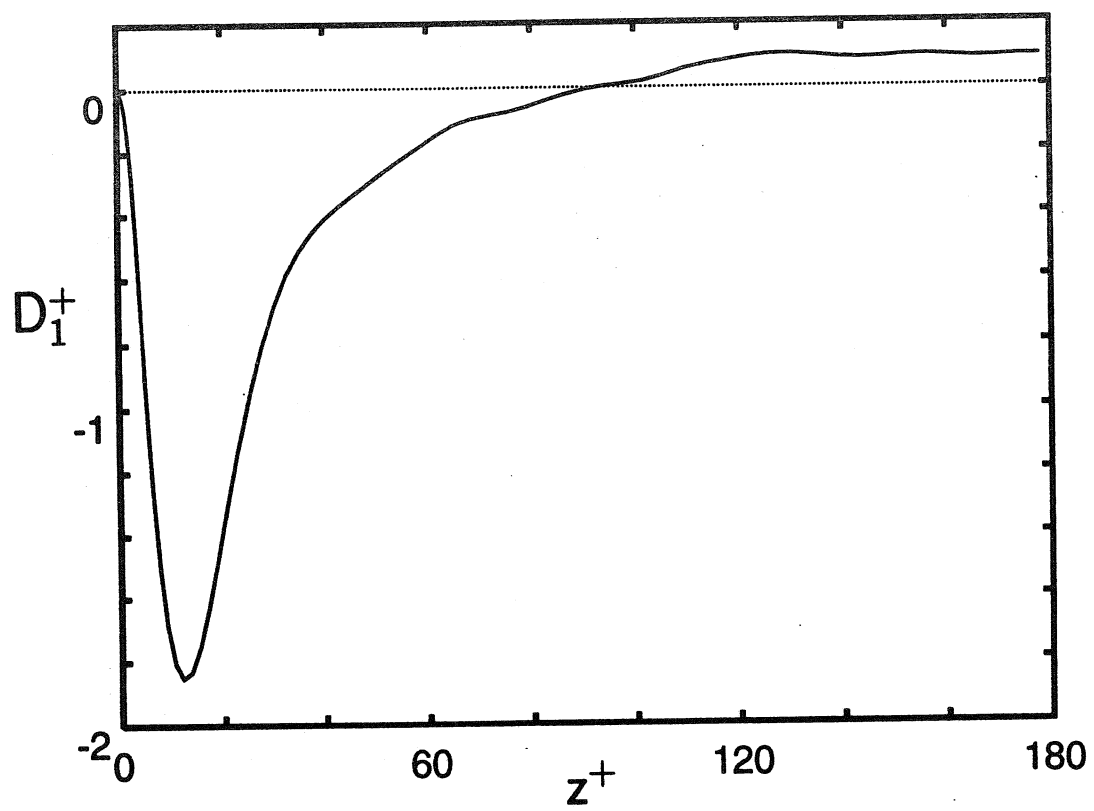


FIG. 11. Plot of the generalized Stokes drift in KH's channel flow.

List of Recent TAM Reports

No.	Authors	Title	Date
846	Lufrano, J. M., P. Sofronis, and H. K. Birnbaum	Elastoplastically accommodated hydride formation and embrittlement— <i>Journal of Mechanics and Physics of Solids</i> , 46 , 1497–1520 (1998)	Feb. 1997
847	Keane, R. D., N. Fujisawa, and R. J. Adrian	Unsteady non-penetrative thermal convection from non-uniform surfaces—In <i>Geophysical and Astrophysical Convection</i> , R. Kerr, ed. (1997)	Feb. 1997
848	Aref, H., and M. Brøns	On stagnation points and streamline topology in vortex flows— <i>Journal of Fluid Mechanics</i> 370 , 1–27 (1998)	Mar. 1997
849	Asghar, S., T. Hayat, and J. G. Harris	Diffraction by a slit in an infinite porous barrier— <i>Wave Motion</i> , 30 , 96–104 (1998)	Mar. 1997
850	Shawki, T. G., H. Aref, and J. W. Phillips	Mechanics on the Web—Proceedings of the International Conference on Engineering Education (Aug. 1997, Chicago)	Apr. 1997
851	Stewart, D. S., and J. Yao	The normal detonation shock velocity–curvature relationship for materials with non-ideal equation of state and multiple turning points— <i>Combustion</i> 113 , 224–235 (1998)	Apr. 1997
852	Fried, E., A. Q. Shen, and S. T. Thoroddsen	Wave patterns in a thin layer of sand within a rotating horizontal cylinder— <i>Physics of Fluids</i> 10 , 10–12 (1998)	Apr. 1997
853	Boyland, P. L., H. Aref, and M. A. Stremler	Topological fluid mechanics of stirring— <i>Bulletin of the American Physical Society</i> 41 , 1683 (1996)	Apr. 1997
854	Parker, S. J., and S. Balachandar	Viscous and inviscid instabilities of flow along a streamwise corner— <i>Bulletin of the American Physical Society</i> 42 , 2155 (1997)	May 1997
855	Soloff, S. M., R. J. Adrian, and Z.-C. Liu	Distortion compensation for generalized stereoscopic particle image velocimetry— <i>Measurement Science and Technology</i> 8 , 1–14 (1997)	May 1997
856	Zhou, Z., R. J. Adrian, S. Balachandar, and T. M. Kendall	Mechanisms for generating coherent packets of hairpin vortices in near-wall turbulence— <i>Bulletin of the American Physical Society</i> 42 , 2243 (1997)	June 1997
857	Neishtadt, A. I., D. L. Vainshtein, and A. A. Vasiliev	Chaotic advection in a cubic stokes flow— <i>Physica D</i> 111 , 227 (1997).	June 1997
858	Weaver, R. L.	Ultrasonics in an aluminum foam— <i>Ultrasonics</i> 36 , 435–442 (1998)	July 1997
859	Riahi, D. N.	High gravity convection in a mushy layer during alloy solidification—In <i>Nonlinear Instability, Chaos and Turbulence</i> , D. N. Riahi and L. Debnath, eds., 1 , 301–336 (1998)	July 1997
860	Najjar, F. M., and S. Balachandar	Low-frequency unsteadiness in the wake of a normal plate, <i>Bulletin of the American Physical Society</i> 42 , 2212 (1997)	Aug. 1997
861	Short, M.	A parabolic linear evolution equation for cellular detonation instability— <i>Combustion Theory and Modeling</i> 1 , 313–346 (1997)	Aug. 1997
862	Short, M., and D. S. Stewart	Cellular detonation stability, I: A normal-mode linear analysis— <i>Journal of Fluid Mechanics</i> 368 , 229–262 (1998)	Sept. 1997
863	Carranza, F. L., and R. B. Haber	A numerical study of intergranular fracture and oxygen embrittlement in an elastic–viscoplastic solid— <i>Journal of the Mechanics and Physics of Solids</i> , 47 , 27–58 (1997)	Oct. 1997
864	Sakakibara, J., and R. J. Adrian	Whole-field measurement of temperature in water using two-color laser-induced fluorescence— <i>Experiments in Fluids</i> 26 , 7–15 (1999)	Oct. 1997
865	Riahi, D. N.	Effect of surface corrugation on convection in a three-dimensional finite box of fluid-saturated porous material— <i>Theoretical and Computational Fluid Dynamics</i> , 13 , 189–208 (1999)	Oct. 1997
866	Baker, C. F., and D. N. Riahi	Three-dimensional flow instabilities during alloy solidification— <i>Bulletin of the American Physical Society</i> 41 , 1699 (1998)	Oct. 1997
867	Fried, E.	Introduction (only) to <i>The Physical and Mathematical Foundations of the Continuum Theory of Evolving Phase Interfaces</i> (book containing 14 seminal papers dedicated to Morton E. Gurtin), Berlin: Springer-Verlag, in press (1998)	Oct. 1997

List of Recent TAM Reports (cont'd)

No.	Authors	Title	Date
868	Folguera, A., and J. G. Harris	Coupled Rayleigh surface waves in a slowly varying elastic waveguide— <i>Proceedings of the Royal Society of London A</i> 455 , 917–931 (1998)	Oct. 1997
869	Stewart, D. S.	Detonation shock dynamics: Application for precision cutting of metal with detonation waves	Oct. 1997
870	Shrotriya, P., and N. R. Sottos	Creep and relaxation behavior of woven glass/epoxy substrates for multilayer circuit board applications— <i>Polymer Composites</i> 19 , 567–578 (1998)	Nov. 1997
871	Riahi, D. N.	Boundary wave-vortex interaction in channel flow at high Reynolds numbers, <i>Fluid Dynamics Research</i> 25 , 129–145 (1999)	Nov. 1997
872	George, W. K., L. Castillo, and M. Wosnik	A theory for turbulent pipe and channel flows—paper presented at <i>Disquisitiones Mechanicae</i> (Urbana, Ill., October 1996)	Nov. 1997
873	Aslam, T. D., and D. S. Stewart	Detonation shock dynamics and comparisons with direct numerical simulation— <i>Combustion Theory and Modeling</i> 3 , 77–101 (1999)	Dec. 1997
874	Short, M., and A. K. Kapila	Blow-up in semilinear parabolic equations with weak diffusion <i>Combustion Theory and Modeling</i> 2 , 283–291 (1998)	Dec. 1997
875	Riahi, D. N.	Analysis and modeling for a turbulent convective plume— <i>Mathematical and Computer Modeling</i> 28 , 57–63 (1998)	Jan. 1998
876	Stremmler, M. A., and H. Aref	Motion of three point vortices in a periodic parallelogram— <i>Journal of Fluid Mechanics</i> 392 , 101–128 (1999)	Feb. 1998
877	Dey, N., K. J. Hsia, and D. F. Socie	On the stress dependence of high-temperature static fatigue life of ceramics	Feb. 1998
878	Brown, E. N., and N. R. Sottos	Thermoelastic properties of plain weave composites for multilayer circuit board applications	Feb. 1998
879	Riahi, D. N.	On the effect of a corrugated boundary on convective motion— <i>Journal of Theoretical and Applied Mechanics</i> , in press (1999)	Feb. 1998
880	Riahi, D. N.	On a turbulent boundary layer flow over a moving wavy wall	Mar. 1998
881	Riahi, D. N.	Vortex formation and stability analysis for shear flows over combined spatially and temporally structured walls— <i>Mathematical Problems in Engineering</i> 5 , 317–328 (1999)	June 1998
882	Short, M., and D. S. Stewart	The multi-dimensional stability of weak heat release detonations— <i>Journal of Fluid Mechanics</i> 382 , 109–135 (1999)	June 1998
883	Fried, E., and M. E. Gurtin	Coherent solid-state phase transitions with atomic diffusion: A thermomechanical treatment— <i>Journal of Statistical Physics</i> 95 , 1361–1427 (1999)	June 1998
884	Langford, J. A., and R. D. Moser	Optimal large-eddy simulation formulations for isotropic turbulence— <i>Journal of Fluid Mechanics</i> 398 , 321–346 (1999)	July 1998
885	Riahi, D. N.	Boundary-layer theory of magnetohydrodynamic turbulent convection— <i>Proceedings of the Indian National Academy (Physical Science)</i> 65A , 109–116 (1999)	Aug. 1998
886	Riahi, D. N.	Nonlinear thermal instability in spherical shells—in <i>Nonlinear Instability, Chaos and Turbulence</i> 2 , 377–402 (1999)	Aug. 1998
887	Riahi, D. N.	Effects of rotation on fully non-axisymmetric chimney convection during alloy solidification— <i>Journal of Crystal Growth</i> 204 , 382–394 (1999)	Sept. 1998
888	Fried, E., and S. Sellers	The Debye theory of rotary diffusion	Sept. 1998
889	Short, M., A. K. Kapila, and J. J. Quirk	The hydrodynamic mechanisms of pulsating detonation wave instability— <i>Proceedings of the Royal Society of London, A</i> 357 , 3621–3638 (1999)	Sept. 1998
890	Stewart, D. S.	The shock dynamics of multidimensional condensed and gas phase detonations— <i>Proceedings of the 27th International Symposium on Combustion</i> (Boulder, Colo.)	Sept. 1998
891	Kim, K. C., and R. J. Adrian	Very large-scale motion in the outer layer— <i>Physics of Fluids</i> 2 , 417–422 (1999)	Oct. 1998

List of Recent TAM Reports (cont'd)

No.	Authors	Title	Date
892	Fujisawa, N., and R. J. Adrian	Three-dimensional temperature measurement in turbulent thermal convection by extended range scanning liquid crystal thermometry— <i>Journal of Visualization</i> 1, 355-364 (1999)	Oct. 1998
893	Shen, A. Q., E. Fried, and S. T. Thoroddsen	Is segregation-by-particle-type a generic mechanism underlying finger formation at fronts of flowing granular media?— <i>Particulate Science and Technology</i> 17, 141-148 (1999)	Oct. 1998
894	Shen, A. Q.	Mathematical and analog modeling of lava dome growth	Oct. 1998
895	Buckmaster, J. D., and M. Short	Cellular instabilities, sub-limit structures, and edge-flames in premixed counterflows— <i>Combustion Theory and Modeling</i> 3, 199-214 (1999)	Oct. 1998
896	Harris, J. G.	<i>Elastic waves</i> —Part of a book to be published by Cambridge University Press	Dec. 1998
897	Paris, A. J., and G. A. Costello	Cord composite cylindrical shells	Dec. 1998
898	Students in TAM 293-294	Thirty-fourth student symposium on engineering mechanics (May 1997), J. W. Phillips, coordinator: Selected senior projects by M. R. Bracki, A. K. Davis, J. A. (Myers) Hommema, and P. D. Pattillo	Dec. 1998
899	Taha, A., and P. Sofronis	A micromechanics approach to the study of hydrogen transport and embrittlement	Jan. 1999
900	Ferney, B. D., and K. J. Hsia	The influence of multiple slip systems on the brittle-ductile transition in silicon— <i>Materials Science Engineering A</i> 272, 422-430 (1999)	Feb. 1999
901	Fried, E., and A. Q. Shen	Supplemental relations at a phase interface across which the velocity and temperature jump	Mar. 1999
902	Paris, A. J., and G. A. Costello	Cord composite cylindrical shells: Multiple layers of cords at various angles to the shell axis	Apr. 1999
903	Ferney, B. D., M. R. DeVary, K. J. Hsia, and A. Needleman	Oscillatory crack growth in glass— <i>Scripta Materialia</i> 41, 275-281 (1999)	Apr. 1999
904	Fried, E., and S. Sellers	Microforces and the theory of solute transport	Apr. 1999
905	Balachandar, S., J. D. Buckmaster, and M. Short	The generation of axial vorticity in solid-propellant rocket-motor flows	May 1999
906	Aref, H., and D. L. Vainchtein	The equation of state of a foam	May 1999
907	Subramanian, S. J., and P. Sofronis	Modeling of the interaction between densification mechanisms in powder compaction	May 1999
908	Aref, H., and M. A. Stremler	Four-vortex motion with zero total circulation and impulse— <i>Physics of Fluids</i> 11, 3704-3715	May 1999
909	Adrian, R. J., K. T. Christensen, and Z.-C. Liu	On the analysis and interpretation of turbulent velocity fields— <i>Experiments in Fluids</i> , in press (1999)	May 1999
910	Fried, E., and S. Sellers	Theory for atomic diffusion on fixed and deformable crystal lattices	June 1999
911	Sofronis, P., and N. Aravas	Hydrogen induced shear localization of the plastic flow in metals and alloys	June 1999
912	Anderson, D. R., D. E. Carlson, and E. Fried	A continuum-mechanical theory for nematic elastomers	June 1999
913	Riahi, D. N.	High Rayleigh number convection in a rotating melt during alloy solidification— <i>Recent Developments in Crystal Growth Research</i> , in press (2000)	July 1999

List of Recent TAM Reports (cont'd)

No.	Authors	Title	Date
914	Riahi, D. N.	Buoyancy driven flow in a rotating low Prandtl number melt during alloy solidification— <i>Current Topics in Crystal Growth Research</i> , in press (2000)	July 1999
915	Adrian, R. J.	On the physical space equation for large-eddy simulation of inhomogeneous turbulence	July 1999
916	Riahi, D. N.	Wave and vortex generation and interaction in turbulent channel flow between wavy boundaries	July 1999
917	Boyland, P. L., M. A. Stremler, and H. Aref	Topological fluid mechanics of point vortex motions	July 1999
918	Riahi, D. N.	Effects of a vertical magnetic field on chimney convection in a mushy layer— <i>Journal of Crystal Growth</i> , in press (2000)	Aug. 1999
919	Riahi, D. N.	Boundary mode-vortex interaction in turbulent channel flow over a non-wavy rough wall	Sept. 1999
920	Block, G. I., J. G. Harris, and T. Hayat	Measurement models for ultrasonic nondestructive evaluation	Sept. 1999
921	Zhang, S., and K. J. Hsia	Modeling the fracture of a sandwich structure due to cavitation in a ductile adhesive layer	Sept. 1999
922	Nimmagadda, P. B. R., and P. Sofronis	Leading order asymptotics at sharp fiber corners in creeping-matrix composite materials	Oct. 1999
923	Yoo, S., and D. N. Riahi	Effects of a moving wavy boundary on channel flow instabilities	Nov. 1999
924	Adrian, R. J., C. D. Meinhart, and C. D. Tomkins	Vortex organization in the outer region of the turbulent boundary layer	Nov. 1999
925	Riahi, D. N., and A. T. Hsui	Finite amplitude thermal convection with variable gravity	Dec. 1999
926	Kwok, W. Y., R. D. Moser, and J. Jiménez	A critical evaluation of the resolution properties of <i>B</i> -spline and compact finite difference methods	Feb. 2000
927	Ferry, J. P., and S. Balachandar	A fast Eulerian method for two-phase flow	Feb. 2000
928	Thoroddsen, S. T., and K. Takehara	The coalescence-cascade of a drop	Feb. 2000
929	Liu, Z.-C., R. J. Adrian, and T. J. Hanratty	Large-scale modes of turbulent channel flow: Transport and structure	Feb. 2000
930	Borodai, S. G., and R. D. Moser	The numerical decomposition of turbulent fluctuations in a compressible boundary layer	Mar. 2000
931	Balachandar, S., and F. M. Najjar	Optimal two-dimensional models for wake flows	Mar. 2000
932	Yoon, H. S., K. V. Sharp, D. F. Hill, R. J. Adrian, S. Balachandar, M. Y. Ha, and K. Kar	Integrated experimental and computational approach to simulation of flow in a stirred tank	Mar. 2000
933	Sakakibara, J., Hishida, K., and W. R. C. Phillips	On the vortical structure in a plane impinging jet	Apr. 2000
934	Phillips, W. R. C.	Eulerian space-time correlations in turbulent shear flows	Apr. 2000
935	Hsui, A. T., and D. N. Riahi	Onset of thermal-chemical convection with crystallization within a binary fluid and its geological implications	Apr. 2000
936	Cermelli, P., E. Fried, and S. Sellers	Configurational stress, yield, and flow in rate-independent plasticity	Apr. 2000